IAC-24,A3,2B,8,x83821

LUMIO: Detecting Meteoroid Impacts on the Lunar Surface

F. Topputo[a], G. Merisio[a], F. Ferrari[a], C. Giordano[a], C. Buonagura[a], A. Martinelli[a], P. Panicucci[a], F. Piccolo[a], A. Rizza[a], E. Peña-Asensio[a], D. Monferrini[b], L. Provinciali[b], L. Pattanaro[b], G. Saita[b], D. Labate[c], M.G. Pancalli[c], G. Cucinella[d], A. Negri[d], A. Locarini[e], A. Morselli[e], L. A. Gomez-Casajus[e], I. Gai[e], A. Quinci[e], A. Thorvaldsen[f], J. Heywood[f], C. Barrack[f], A. Cervone[g], D. Koschny[h], E. Ammannito[i], R. Moissl[l], R. Walker[h]

[a] *Department of Aerospace Science and Technology, Politecnico di Milano, Via La Masa 34, 20156, Milano, Italy*
[b] *Argotec Srl, Via Cervino 52, 10155, Torino, Italy*
[c] *Leonardo, Via delle Officine Galileo 1, 50013, Campi Bisenzio, Italy*
[d] *IMT Srl, Via C. Faccinetti 67, 00159, Roma, Italy*
[e] *Nautilus – Navigation in Space Srl, Via G. Fanin 48, 40127, Bologna, Italy*
[f] *Science and Technology AS, Tordenskiolds Gate 3, 0160, Oslo, Norway*
[g] *Delft University of Technology (TU Delft), Kluyverweg 1, 2629, Delft, The Netherlands*
[h] *European Space Agency (ESA), ESTEC, Keplerlaan 1, 2201 AZ, Noordwijk, The Netherlands*
[i] *Italian Space Agency (ASI), Via del Politecnico snc, 00133 Roma, Italy*
[l] *European Space Agency (ESA), ESOC, Robert-Bosch-Str. 5, 64293 Darmstadt, Germany*

Abstract

Lunar meteoroid impacts have caused in the past a substantial change in the lunar surface. With no atmospheric shield, the Moon is subject to many impacts from meteoroids, ranging from a few grams to a few kilograms. The high impact rate on the lunar surface has important implications for future human and robotic assets that will inhabit the Moon for significant periods of time. Therefore, a better understanding of the meteoroid population in the cislunar environment is required for future exploration of the Moon. Moreover, refining current meteoroid models is of paramount importance for many applications, including planetary science investigations. Studying meteoroid impacts can help deepening the understanding of the spatial distribution of near-Earth objects in the Solar System. The ability to predict impacts is therefore critical to many applications, both related to engineering aspects of space exploration, and to more scientific investigations regarding evolutional processes in the Solar System. The Lunar Meteoroid Impacts Observer (LUMIO) is a CubeSat mission to observe, quantify, and characterise lunar meteoroid impacts, by detecting their impact ashes on the far-side of the Moon. This complements the information available from Earth-based observatories, which are bounded to the lunar near-side, with the goal of synthesising a global recognition of the lunar meteoroid environment. LUMIO envisages a 12U CubeSat form-factor placed in a halo orbit at Earth-Moon L2. The detections are performed using the LUMIO-Cam, an optical instrument capable of detecting light ashes in the visible spectrum (450-950 nm). LUMIO has successfully passed the PDR and is currently moving towards Phase C. We present the latest results on the modelling of the meteoroid environment in the Earth-Moon system, including an estimate of LUMIO's potential impact on our existing knowledge of meteoroids, supported by high-fidelity simulation data. An overview of the present-day LUMIO CubeSat design is also given, with a focus on the latest developments involving both the ongoing/planned scientific activities and the development of the payload.
Keywords: LUMIO, lunar meteoroid, CubeSat, Moon

1. Introduction

LUMIO is a 12U CubeSat mission to a halo orbit at Earth–Moon L_2 that shall observe, quantify, and characterize meteoroid impacts on the lunar far side by detecting their impact flashes, complementing Earth-based observations on the lunar nearside, to provide global information on the lunar meteoroid environment and contribute to Lunar Situational Awareness.

- **Rationale**: An accurate meteoroid flux model in the Lunar environment is fundamental for future humans' outposts on the Moon. Ground-based telescopes cannot observe the Moon far-side, thus scientific information is missing.
- **Scientific Question**: What are the spatial and temporal characteristics of meteoroids impacting the lunar surface?
- **Scientific Goal**: To characterize how meteoroids evolve in the cislunar space by observing the flashes produced by their impacts with the lunar surface.
- **Scientific Objective**: To conduct observations of the lunar surface to detect meteoroids impacts and characterise their flux, magnitudes, energies, and sizes.
- **Tech-demo Objective** To demonstrate use of miniaturized technologies, CubeSat operations, and autonomous systems in lunar environment.

1.1 Phase B summary

Science: To synthetize a solar system meteoroid flux model by detecting their impact flashes on the Moon far side.

Payload: LUMIO-Cam:

- Visible/Infrared
- Impacts Detection
- 6 deg FOV
- 15 fps
- Onboard processing

Fig. 1. LUMIO-Cam

Operative Orbit: Quasi-halo orbit about Earth-Moon L_2 point:

- ~ 2:1 resonance with E-M period
- Repetitive operations
- Permanent lunar far-side observation
- Earth always in sight

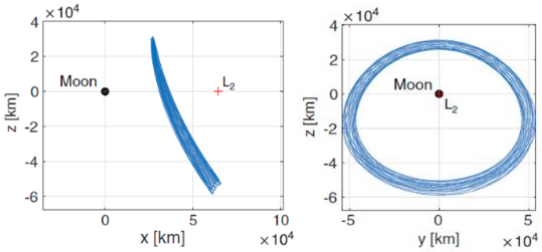

Fig. 2. LUMIO quasi-halo operational orbit

Platform: Deep-space CubeSat:

- Size: 12U
- Mass: ~ 28 kg
- Power: ~ 60 W
- Delta-v: ~ 80 m/s
- Lifetime: 1.5 years

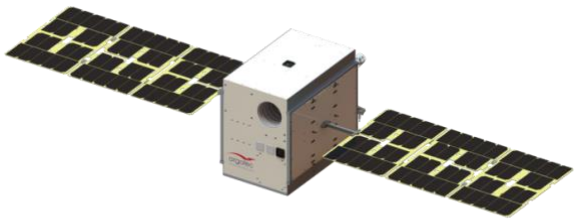

Fig. 3. The LUMIO CubeSat

2. Scientific Motivations

2.1 Relevance

Impacts due to near Earth objects could cause a devastating humanitarian crisis and potentially the extinction of the humans. While the probability of such an event is low, the outcome is so catastrophic that it is imperative to invest resources to mitigate them. Telescopic surveys detect NEOs > 1 km down to 1 meter, but there are few direct methods for monitoring the sub-meter meteoroid population. Meteoroids are small Sun-orbiting fragments of asteroids and comets, whose sizes range from micrometers to meters and masses from 10^{-15} to 10^{4} kg [1]. Their formation is a consequence of asteroids colliding with each other or with other bodies, comets releasing dust particles when close to the Sun, and minor bodies shattering into individual fragments. Meteoroids are hardly detectable even with dedicated surveys. However, they may be observed indirectly when an impact occurs with a planetary or moon solid surface. The ability to accurately predicting these impacts by relying on accurate meteoroid impact flux models is fundamental.

2.2 Lunar meteoroid impacts

Current estimations of the larger-than-1-kg meteoroid flux at the Moon varies across the literature. The model in [2] estimates 1290 impacts per year, while the one in [3] estimates approximately 4000 impacts per year [4]. More recent studies suggest that the meteoroid impact flux at the Moon is approximately 6 10^{-10} m^2/year, for meteoroids larger than 30 grams [5]. Assuming a lunar collecting area equal to its surface area, 3.8 10^{13} m^2, this gives a larger-than-30-grams meteoroid flux of approximately 23,000 impacts per year. There are also speculations on the possible asymmetries of the spatial distribution of impacts across the lunar surface. In [6], it is theorized that the Moon nearside has approximately 0.1% more impacts than the lunar farside, due to the Earth gravity field; the equatorial flux is 10–20% larger than that at polar regions, due to the higher number of large meteoroids in low orbital inclinations; and the lunar leading side (apex) encounters between 37% to 80% more impactors than the lunar trailing side (antapex), due the Moon synchronous rotation. In a lunar meteoroid impact, the kinetic energy of the impactor is partitioned into 1) the generation of a seismic wave, 2) the excavation of a crater, 3) the ejection of particles, and 4) the emission of radiation. Any of these phenomena can be observed to detect lunar meteoroid impacts. The detection of lunar impact flashes is the most advantageous method since it yields an independent detection of meteoroid impacts, provides the most complete information about the impactor, and allows for the monitoring of a large Moon surface area. Remote observation of light flashes is thus baselined for the detection of lunar meteoroid impacts.

2.3 Sun–Earth–Moon geometry

The Moon spin–orbit motion is locked into a 1:1 resonance, meaning that an observer on Earth always sees the same portion of the Moon, that is, the lunar nearside. This characteristic, in addition to the fact that a fixed observer on Earth also moves with respect to the Moon, as the Earth rotates about its own axis, constrain the observation of the Moon from the Earth. Since the Moon–Sun synodic period is 29.53 days, the illumination of the lunar nearside varies, which originates the Moon phases. Because lunar impact flashes can only be observed from ground on the lunar nightside and when the lunar nearside is less than 50% illuminated, their detection from Earth is constrained by this Sun–Earth–Moon geometry. Observing the lunar impacts with space-based assets yields several benefits over ground-based telescopes, namely:

- *No atmosphere*. Ground-based observations are biased by the atmosphere that reduces the light flash intensity depending upon present conditions, which change in time. This requires frequent recalibration of the telescope. With the absence of atmosphere in space-based observations, there is no need of recalibrating the instrument and fainter flashes can be detected.
- *No weather*. Ground-based observations require good weather conditions, the lack of which may significantly reduce the observation time within the available window. There is no such constraint in space-based observations.
- *No day/night*. Ground-based observations may only be performed during Earth night, significantly reducing the observation periods. There is no such limitation when space-based observations are performed.
- *Full disk*. Ground-based observations are performed in the first and third quarter, when nearside illumination is 10–50%. Full-disk observations during New Moon are not possible because of low elevation of the Moon and daylight. Space-based observations of the lunar farside can capture the whole lunar full-disk at once, thus increasing the monitored area.
- *All longitudes*. Ground-based observations in the first and third quarter prevent resolving the meteoroid flux across the central meridian. There is no restriction in space-based observations.

Moreover, observing the lunar farside with space-based assets yields further benefits, which are the absence of earthshine and the complementarity of observations with respect to the ground-based ones. The absence of Earthshine yields a lower background noise, thus enabling the detection of fainter signals, not resolvable from ground. Then, space-based observations of the lunar farside complement ground-based ones in space and time. In space, the two opposite Moon faces are monitored when the Moon is in different orbit locations, while in time, observations are performed in periods when ground-based ones are not possible.

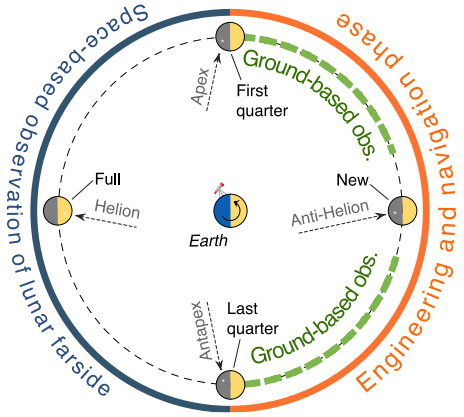

Fig. 4. Moon phases and main directions of incoming meteoroids in the Earth-Moon system. The dashed green line represents the portion of the Moon orbit where Earth-based observations of the nearside can be made. The solid blue line indicates when space-based observations of the lunar far side can be made. The solid orange line indicates the periods for other operations.

2.3 Lunar Meteoroid Impact Flash Detection

Light flashes at the Moon are observed by detecting a local spike of the luminous energy in the visible spectrum when pointing a telescope at the lunar nightside. The background noise is mainly composed by the Earthshine in the visible spectrum, and by thermal emissions of the Moon surface in the infrared spectrum [7]. Measurements with high signal-to-noise ratios can be obtained through observations of the lunar nightside [8]. The detected luminous energy spike is quantified using the apparent magnitude of the light flash. Lunar impact flashes detected from Earth-based observations have apparent magnitude between +5 and +10.5 [6], which correspond to very faint signals. Also, Earth-based observations of lunar impact flashes are restricted to periods when the lunar nearside illumination is 10–50% [3], [9]. The first unambiguous lunar meteoroid impact flashes were detected during 1999's Leonid meteoroid showers and were reported in [8]. The first redundant detection of sporadic impacts was only reported six years later in [3]. These events gave origin to several monitoring programs. In 2006, a lunar meteoroid impact flashes observation programme was initiated at NASA Marshall Space Flight Center [9]. This facility can monitor 4.5 10^6 km^2 of the lunar surface, approximately 10 nights per month, subject to weather conditions. The most recent monitoring program, NELIOTA, was initiated on February 2017 in Greece under ESA funding. The program aims to detect flashes as faint as +12 apparent visual magnitude [10] and is the first allowing the determination of the impact

flash blackbody temperature, by observing both in the visible and infrared spectrum. Monitoring the Moon for impact flashes imposes several restrictions that can be avoided if the same investigation is conducted with space-bases assets.

3. Impact flash detector: the LUMIO-Cam

In the LUMIO mission, the observation of the light flashes produced by meteoroid impacts on the Moon far side is performed through the main payload, which is the LUMIO-Cam. The instrument operates between 450 and 950 nm, implementing a double Focal Plane Assembly configuration.

3.1 Payload requirements

The impact flashes on the Moon can be modelled as black body emissions [6], with temperatures between 2700 K and 6000 K [7], and durations greater than 30 ms [5]. The lowest impact energies correspond to apparent magnitudes higher than 6 as seen from Earth. These characteristics drive the payload requirements, whose high-level ones are listed in Table 1.

Table 1. LUMIO payload high-level requirements

ID	Requirement
PLD.001	The payload shall detect flashes with energies between 10^{-6} and 10^{-4} kT TNT.
PLD.002	The payload shall detect flashes in the radiation spectrum between 450 nm and 950 nm.
PLD.003	The image integration time shall be equal or greater than 30 ms.
PLD.004	The mass of the payload shall be no more than 4.5 kg.
PLD.005	The maximum power consumption of the payload shall be no more than 20 W.
PLD.006	The maximum size of the payload shall be 10 cm x10 cm x 30 cm.

3.2 Detectors

The LUMIO-Cam uses two detectors, one in the visible band and one in the near infrared band. A dichroic cube has been positioned before the two detectors to split the radiation at 820 nm, enabling the correlation of the impact flashes acquired both in the VIS and NIR band. Having a second measurement in the NIR band will allow reconstructing the temperature of the impact flash based on the ratio between the two observations' magnitude in both VIS and NIR band. Two identical 1024x1024 CCD detectors, namely the CCD201-20 developed by E2V-Teledyne, are positioned after the dichroic cube, shifted by 90 degrees. The detector is a 1024x1024 pixel frame-transfer capable of operating at an equivalent output noise of less than one electron at pixel rates of over 15 MHz. This makes the sensor well-suited for scientific imaging where the illumination is limited and the frame rate is high, as it is for LUMIO. The detector features are reported in Table 3.

Table 2. CCD201-20 detector features

Parameter	Value
Image Area	13.3 mm x 13.3 mm
Active Pixels	1024 x 1024
Pixel Size	13.3 μm x 13.3 μm
Storage Area	13.3 mm x 13.3 mm
Low Noise Gain	1 – 1000
Readout Frequency	15 MHz
Charge Handling Cap.	80ke$^-$/pixel
Readout Noise	< 1 e$^-$ rms

3.3 Optics

Considering the LUMIO orbit (Section 4), for which the S/C-Moon range spans between 35000 and 85000 km, a minimum payload field of view (FOV) of 5.68 deg is necessary to always have the Moon full disk view. To compensate for pointing errors and other effects, a 6 deg FOV is considered for the LUMIO-Cam, leading to a 127 mm focal length and an aperture of 51 mm.

3.4 Mechanical layout

The mechanical layout of the LUMIO-Cam is shown in Fig. 1. It includes a mechanical barrel supporting five lenses, an entrance baffle for out-of-field straylight reduction, two focal plane assemblies, a proximity electronics box, and an external box for mechanical protection. Overall, the instrument dimensions are within 300 mm x 100 mm x 100 mm.

3.5 Budgets

The mass budgets are reported in Table 5.

Table 3. Payload mass budget

Subassembly	Mass [kg]	Mass w/ margin [kg]
Optical Head & Focal Plane	1.87	2.35
Proximity Electronics	1.25	1.50
TOTAL	**3.12**	**3.85**

LUMIO-Cam power budget has been evaluated taking into account the following assumptions:

- 2 heaters (coupled with each CCD) with maximum consumption of 3000 mW each.
- 75% of DC/DC converter efficiency (worst case)
- Detector operating @ 15MHz (as reported in datasheet)

The current maximum worst case power consumption is equal to **27.8 W** (heaters included).

4. Mission Analysis

The Earth–Moon L2 halo family is baselined for the LUMIO mission, after a detailed trade-off of orbit options involving scientific return, safety, coverage, and

cost as guiding criteria. It has been shown that remotely detecting flashes on the lunar surface from the halo orbit family is the only technically and economically viable option for a CubeSat [11]. The LUMIO mission, as graphically shown in Figure 3, is divided in 5 phases:

(1) Launch and Early Operations Phase (LEOP)

(2) Commissioning phase

(3) Transfer phase

(4) Operative phase,

(5) End-of-Life phase.

In LEOP (1), LUMIO is switched off inside the deployer. The LEOP ends when the carrier executes a Trans Lunar Injection (TLI), which places LUMIO into a Weak Stability Boundary (WSB) transfer toward the Moon. During the Commissioning phase (2) the following operations are accomplished: LUMIO is released; De-tumbling; Deployment of the solar arrays; Commissioning of all subsystems; Direct-with-Earth (DWE) link for communication. Then LUMIO enters in the Transfer phase (3), where it is expected to use its own propulsion system. Several transfer maneuvers are expected: several Deep Space Maneuvers (DSM) (2 on average) and a final Halo Injection Maneuver (HIM). The Transfer phase ends when the operative orbit is reached, and the HIM is executed. Then, LUMIO enters in the Operative phase (4), where the operative halo orbit is divided in two cycles: the scientific cycle for continuous processing of images and the engineering cycle for station keeping and platform life checks and corrections. Eventually, after 1 year of operations, LUMIO enters in the End-of-Life phase (5) with a disposal maneuver to target a crash on the Moon.

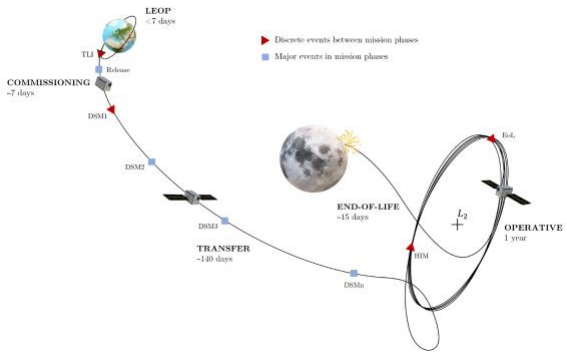

Fig. 5. LUMIO mission phases

4.1 Earth-Moon L2 quasi-halo orbit

The quasi-periodic halo orbit about Earth–Moon L2 characterized by a Jacobi constant Cj = 3.09 is the designated LUMIO operative orbit (Fig. 6). The selection of LUMIO operative orbit energy is the result of a thorough trade-off analysis performed during the Phase 0 design [11].

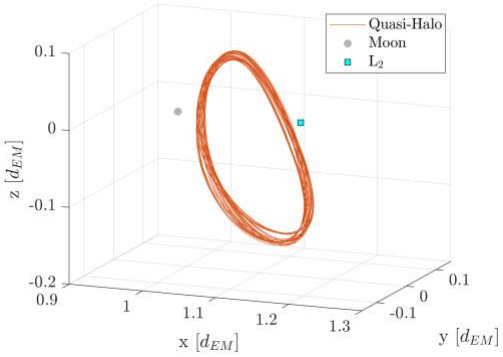

Fig. 6. LUMIO operative orbit

4.2 Weak Stability Boundary transfer

LUMIO is released along the WSB transfer by a primary mission. The mothercraft is considered to go to low-lunar orbit (orbiter or lander), following a trajectory called Layer 1. Once released, LUMIO will follow instead a trajectory called Layer 2, which will bring the spacecraft to the operative quasi-halo orbit. Both layers are computed and optimized for each week of the 2027.

For Layer 1, it is assumed that the trajectory of the mothercraft departs from a Low Earth Orbit (LEO) having an altitude of 200 km, while the target orbit is an LLO with a pericenter altitude of 100 km. The only maneuvers considered for this layer are the TLI and a final injection on the target LLO. Following the methodology in [21], the computation of the first layer is performed to seek a solution for each of the 52 weeks in 2027. Once a solution is found for that epoch, a continuation scheme is used to shift a transfer of the same family to a different departure epoch. At the end, a total of 104 trajectories are found for the Layer 1. The optimal cost for these solutions ranges between 3.83km/s and 3.86km/s, which, as expected, is lower than the cost of an Earth–Moon Hohmann-like transfer (>3.9km/s), while the time of flight can vary between a minimum of 85 d to a maximum of 130 d. Interested readers can refer to [21] for more details.

Layer 2 represents the trajectory that LUMIO will actually follow. LUMIO is expected to be released by the mothercraft 0.5 days after the TLI. The release mechanism is expected to impress a Δv_R of 1.5 m/s to LUMIO to separate it from the main spacecraft. From this point on, LUMIO will rely only on its propulsion to further separate its own trajectory from the one of the first layer. This will be possible thanks to a maximum of 8 DSMs, that will guide LUMIO to the final Halo Insertion Maneuver (HIM).

The results of the optimization are shown in Fig. 7 where the total Δv needed for each week of the year considering the best solution is shown. From the figure

it is possible to see an annual trend: the average cost indeed oscillates over 40 m/s, even though the weekly variations are relevant. This is due to the variability of the first layer, whose trajectories differ considerably between each other.

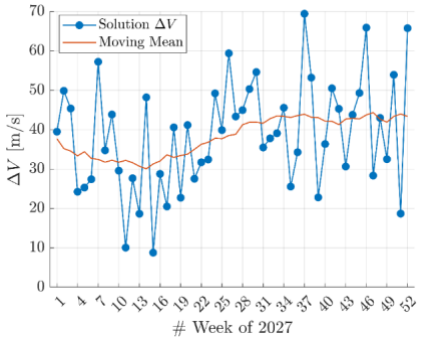

Fig. 7. Transfer Δv for layer 2 solutions

The trajectory associated with the week 20 of 2027, which departs on May 19, 2027, is the baseline chosen for LUMIO. The trajectory can be seen in Fig. 8. The transfer requires only 2 DSMs, DSM-3 and DSM-4, which are located around the apogee, to minimize their cost. After the DSM-4, performed 44.85 d after the TLI, LUMIO will follow the stable manifold for ~50 d, until the small insertion maneuver on the quasi-halo.

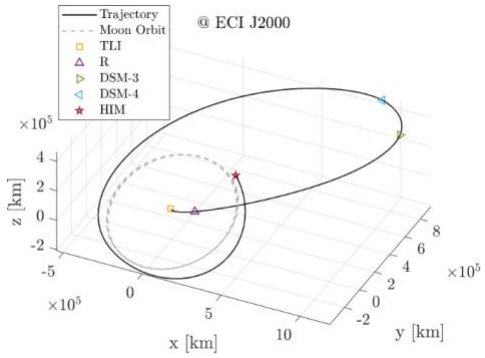

Fig. 8. Baseline transfer trajectory

More details on the LUMIO mission analysis are available in [22].

4.3 Station-keeping on quasi-halo orbit

Considering the limited Δv capability, fuel consumption for station-keeping around the operative orbits will be a critical factor for mission sustainability. The S/K cost is estimated by employing the *target points method* (TPM) first introduced in [14], then adapted to the problem of LPOs [15], and finally used for JAXA's EQUULEUS mission analysis [16]. A massive Monte-Carlo simulation is performed considering the impact of the injection, tracking, and maneuver execution processes on the nominal orbit determined. The estimated the 1-year S/K cost has a mean of 8.256 m/s and 3-σ of 15.79 m/s, considering a cut-off time of 2 days before the maneuver.

4.4 Delta-V budget

The mission Δv budgets for each maneuver required to reach the operative orbit and cost for station keeping along the operative orbit are reported in Table **4**.

Table 4. Mission delta-V budget

Maneuver	Deterministic [m/s]	Stochastic (3σ) [m/s]	Margin (5%) [m/s]
DSM 1-8	40.85	10.22	2.55
TCM 1-7	-	7.08	0.35
HIM	0.32	0.06	0.02
1-year S/K	-	15.79	0.79
Disposal	0.97	-	0.05
TOTAL			**79.05 m/s**

5. Optical navigation experiment

LUMIO proposes to run an autonomous navigation experiment. In the context of the LUMIO mission, the limb-based optical navigation is selected as the Moon lit limb is clearly visible in the image. The overall process implemented to simulate LUMIO autonomous navigation consists of:

- The generation of synthetic Moon images with a rendering software
- The processing of these images for limb-based navigation
- The determination of the spacecraft state via extended Kalman filter.

The Vision-Based Navigation (VBN) algorithm is divided in two main parts: The image processing (IP) and the navigation filter. The image processing computes the Moon-spacecraft position in the Moon reference frame, whereas the navigation filter processes this observable to estimate the spacecraft state. This is performed by extracting coarse estimate of the limbs and by refining them in an increasing accuracy process. The output of the limb point determination extract points of the limb with 0.2 pixel accuracy as reported in Fig. 9. Lim points are the used to determine the position of the spacecraft with respect to the Moon by fitting a spherical Moon over the determined circle on the image. More details are available in [23] and [24].

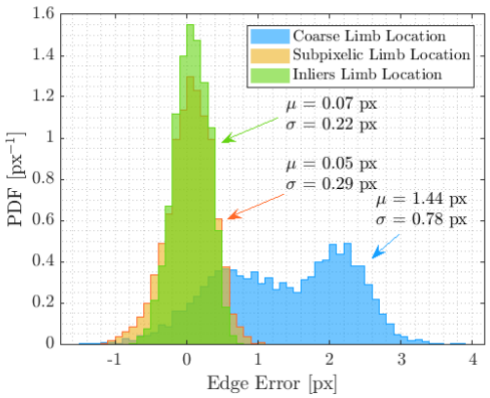

Fig. 9. Error of the detected limb points at different stages of the IP

The output of the IP algorithm is the camera-to-Moon position estimation in the camera reference frame, yet no information on spacecraft velocity is available. An extended Kalman filter (EKF) is then used to estimate the spacecraft state (e.g., position and velocity), and to increase the navigation accuracy. The on-board EKF estimates the state of the spacecraft in a J2000 reference frame centred in the Earth-Moon barycentre. The results in terms of position and velocity in the camera frame for the Monte Carlo simulation of the first scenario are reported in Fig. 10.

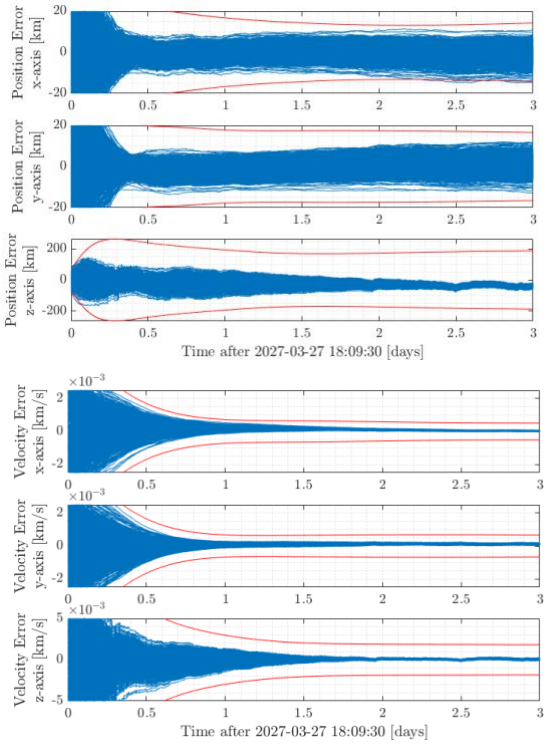

Fig. 10. The Monte Carlo results in terms of position and velocity error in the camera frame for the first three days after the beginning of the first Nav&Eng Cycle.

The filter converges rapidly despite the spacecraft is orbiting in the more non-linear part of the orbit. This is due to the accuracy and precision of the image processing measurements. The position is estimated with an error below 100 km for the z-axis and 10 km for the x-axis and y-axis. Moreover, the covariance bounds are below 200 km for the z-axis and 20 km for the x-axis and y-axis. This is consistent with vision-based navigation techniques that can provide accurate measurement in the image plane, while less precise orbit determination on the camera boresight. The velocity is well determined as well with an error below 1 m/s for the z-axis and 0.5 m/s m for the x-axis and y-axis. the velocity covariance bound converges to about 4 m/s for the z-axis and 1.5 m/s m for the x-axis and y-axis.

6. System

The LUMIO spacecraft has been designed to perform with a high level of autonomy, particularly for the payload data processing. This choice was driven not only by the operational constraints involved with the observation of the flashes, but also by the ambitious mission design. Additionally, a general zero-redundancy approach has been adopted for all subsystems. This is dictated by the tight mass and volume constraints and a CubeSat design driven risk approach. In subsystem design, a systematic trade-off procedure has been adopted, based on subsystem specific performance criteria, as well as standard performance, cost and schedule criteria. Consistent design margins have been used for sizing the subsystems based on the development status. A standard 5, 10 and 20% mass margin has been applied for a fully COTS solution, a COTS solution requiring modification and a custom design, respectively. The most important system and sub-system requirements are summarized in Table 11.

Table 5. Main system and subsystem requirements

ID	Requirement
SYS-01	The mass of the spacecraft shall not be greater than 28 kg.
SYS-02	The spacecraft volume shall not exceed that of a 12U CubeSat.
SYS-03	The satellite shall be able to operate in Lunar environment for at least 1 year.
PROP-01	The propulsion system shall provide a minimum ΔV = 80 m/s for station keeping, orbital transfer, and end-of-life disposal.
PROP-02	The propulsion system shall have a wet mass of no more than 6 kg.
PROP-03	The propulsion system shall have maximum thrusting time of 1 hour per orbital transfer maneuver.
PROP-04	The RCS propulsion system shall provide a Total Impulse for all RCS tasks of 110 Ns.
ADCS-01	The spacecraft shall provide an absolute performance error of better than 0.18 deg half-cone during Moon pointing for scientific acquisitions.
ADCS-02	The spacecraft shall provide a relative performance error of better than 5 arcsec over 66.7 ms during Moon pointing for scientific acquisitions.
ADCS-03	The ADCS shall provide a maximum slew rate of 0.5 deg/s.
EPS-01	The EPS shall have a power generation larger than 53.8 W average and a peak power capability of 68 W.

EPS-02	The EPS shall have a mass no more than 3 kg.
COM-01	The spacecraft shall be able to receive commands for more than 95% of all spacecraft orientations in all operational scenarios.
COM-02	The spacecraft telemetry shall be receivable for more than 95% of all spacecraft orientations in all operational scenarios.
COM-03	The communication system shall provide radio navigation support with a position accuracy of 1 km 3-sigma.
PLDP-01	The payload processor shall receive and process at least 15 images per seconds from the payload.
PLDP-02	The payload processors shall identify flashes with SNR greater than 5 dB.
TCS-01	The TCS shall guarantee a temperature range for the payload between -20 deg C and + 50 deg C.
TCS-02	The TCS shall guarantee a temperature range for the internal parts of the system between -10 deg C and + 50 deg C.

6.1 Propulsion

The propulsion system for LUMIO comprehends two systems, the Main Propulsion System and the Reaction Control System. The MPS is responsible for the orbital maneuvering, while the RCS is used for MPS torque compensation and desaturation of the reaction wheels. An initial trade-off for the main propulsion system has been performed during the LUMIO phase A study. The trade-off criteria were the thrust level, mass, volume, power, schedule/TRL, cost, and compliance with propulsion requirements. It has been found that the mono propellant is the only type of propulsion able to meet all the propulsion requirements for LUMIO. A monopropellant blow-down MPS designed by Bradford during the Phase B, whilst Lift Me Off will be performing the detailed design and development of the system in Phase C/D. The system budgets given in this paper are based on the Phase B baseline, and are therefore subject to change. It employs LMP-103S as propellant and helium as a pressurizing agent, which are stored jointly in the same tank and separated by an internal diaphragm. The MPS is equipped with one single thruster, the ECAPS 1N High Performance Green Propellant (HPGP) Rocket Engine, located in the central tunacan.

Similarly to what was done for the main propulsion, an initial trade-off was performed for the RCS propulsion to define which type(s) of propulsion would be the most suitable for the task. The trade-off criteria were the thrust level, mass, volume, power, schedule/TRL, cost, and compliance to other requirements. The chosen RCS is a cold gas system which exploits the refrigerant R134a as a propellant. R134a is a two-phase fluid existing in liquid phase and vapor phase simultaneously. Using a refrigerant as a propellant is beneficial as it can be stored in a smaller tank volume compared to other gaseous cold gas propellants. To eject the propellant in gaseous state, the biphase propellant goes through a phase transition in the vaporizer and reaches the vapor tank in vapor phase where it is stored prior to the RCS firing. The RCS employs 4 thrusters to ensure the 3-axis spacecraft control.

6.2 Attitude determination and control

The XACT-100 was selected as the baseline ADCS for the LUMIO mission. It offers high performance and reliability maintaining a minimal form-factor. This offers a significant heritage. with several deep space missions that have used the XACT successfully. (e.g., MARCO, Lunar Icecube, Lunar Flashlight, CUSP, Bionsentinel, Equuleus, Argomoon and LICIACube).

The XACT-100 is composed by a 0,5U main box with the following equipment: a dedicated ADCS electronic control board. star trackers and gyroscopes. The external equipment, connected directly to the main ADCS box, is composed of one external reaction wheel, external Sun Sensors and one additional external Star Tracker.

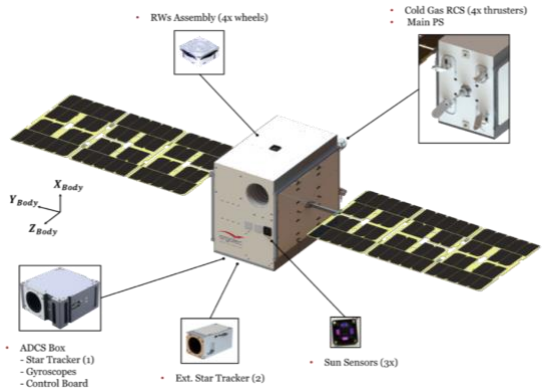

Fig. 11. ADCS architecture of the LUMIO spacecraft

Three external RWp100 and one external RWp050 are considered as the baseline. Each reaction wheel RWp100 provides a momentum capacity of 100mNms, whereas the RWp050 provides a momentum capacity of 50mNms. The three RWp100 are aligned with the spacecraft body axis while the RWp050 is tilted to distribute evenly the momentum on the three body axes. This ensures to project the RW rotation axis equally on the spacecraft principal axes. This configuration was selected to respect the volume constraints on the spacecraft, despite the reduced overall momentum stored with respect to a pyramid configuration. The Standard NST Star Tracker maintains a valid attitude up to a rate of 2 deg/s; if this value is exceeded the ADCS enters automatically in the Sun Point mode. Considering that a single star tracker represents a single point of failure for the mission, a second star tracker is baselined. The XACT includes a set of gyroscopes to measure the spacecraft angular rate along the three body axes of the SC. During the mission the information provided by the gyros, combined with the measurements from the star tracker, are essential to retrieve the attitude

of the platform. During the detumbling instead, when the angular rate exceeds the operative limit of the star tracker (< 2 deg/s), the gyroscopes are the solely sensors exploited for the attitude determination. Table 6 shows the estimated pointing performances stressing the different source of noises affecting the pointing budget. These values are in line with the performance declared by the manufacturer and are compliant with the LUMIO pointing requirements.

Reaction wheels desaturation is performed using the RCS described in the previous section. The momentum budget computed on the full mission profile leads to a total impulse of 170 s, including contribution due to nominal pointing profile and thruster misalignment compensation.

Table 6. XACT estimated pointing performance

Pointing Error Sources	Type	3σ (arcsec)		
		x	y	z
ADCS pointing error (ST+RWs+Controller)	Gaussian	75.6	32.4	32.4
Payload Misalignment	Bias	240	240	240
Star Tracker Misalignment	Bias	72.0	72.0	72.0
ST Thermo-Elastic Distortion	Harmonic	95.5	94.3	89.7
Payload Thermo-Elastic Distortion	Harmonic	102.3	98.0	97.2
Position Knowledge	Harmonic	17.1	17.1	17.1

6.3 Power

The Electrical Power System (EPS) is composed of three main components: the Solar Panel Array (SPA), the Battery (BAT) and the Power Conditioning and Distribution Unit (PCDU).

The IMT µSADA is a Solar Array Drive Assembly suitable for CubeSAT and Deep Space Mission (Figure 9). It is composed by an internal unit, called SADU, the HDRM system and two Solar Arrays. The internal unit is the mechanical and electronical equipment needed for the Solar Array rotation. The HDRM is based on a thermal cutter system and the two solar arrays are composed by three foils each one. Thanks to the slip ring assembly, inside the SADU, it is possible to rotate the solar panels several turns without any cable saturation.

The baseline PCDU for the LUMIO mission is a reworked version of the Argotec Volta PCDU. Such rework is performed to ensure the compatibility with all the subsystems and the power requirements while maintaining its reliability and features.

A Maximum Power Point Tracking (MPPT) algorithm to optimize the power coming from the Solar Panels and a Battery Charging Regulation (BCR) system to charge the battery are implemented autonomously by the Volta PCDU, without requiring any external control.

The secondary power rails of the Volta PCDU are compatible with the power supply requested by each subsystem. Each line is protected against Over-Current, Over-Voltage, and Under-Voltage. The Volta PCDU provides Retriggerable Latching Current Limiter protection able to counteract the Single Event Effects on other subsystems.

The baseline battery is the 7S2P Li-ion ABSL124Wh. The topology of two cells strings allows to have a more reliable battery, and the 7 cells in each string allow the connection of the battery directly to the main bus of the PCDU, since they operate at the standard voltage of 28V. This battery is fully compatible with the PCDU as already demonstrated in the LICIACube and ArgoMoon missions. This means that it was already tested and flown in the deep space environment.

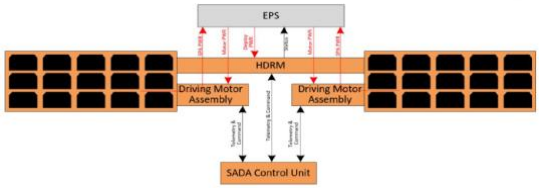

Fig. 12. µSADA architecture diagram

6.4 Communication

LUMIO is expected to have a Direct-To-Earth (DTE) link. The DTE link is using a traditional configuration with one ground station (to limit mission cost, even though multiple stations can be considered, if needed) communicating directly with LUMIO. To this aim, an X-band link will be set to allow for telecommands, payload data downlink, ranging, and tracking in nominal conditions. The radio selected is the IMT C-DST, and two patch antennas have been considered.

6.5 Structure and thermal

The LUMIO structure is a custom design by Argotec based on the 12U standard. Full compliance with the standard is not achieved due to the lateral protrusion of the spacecraft which are adopted to increase internal available volume. The spacecraft structure is divided into a Primary Structure (rails, side frames, ribs) providing global stiffness to the Platform, a primary interface to the Deployer and interfaces to all the subsystems, and a Secondary Structure (radiator panels, mounting elements). The chosen material is Aerospace Al 7075 T7351, as it offers the best combination in terms of limit stress and manufacturability.

The TCS is designed to use as few active techniques as possible in order to increase the system reliability. The only active techniques so far present are represented by heaters.

6.5 Command and data handling system

The baseline OBC for the LUMIO mission is a slightly reworked version of the Argotec Fermi OBC. The minor rework only concerns the addition of a CAN bus transceiver and the usage of MRAMs instead of EEPROMs as boot memories.

Flexibility in the processing algorithms is provided by a hybrid architecture based on two main radiation hardened components: CPU and FPGA.

6.7 Spacecraft configuration and budget

Figure 13 shows the current foreseen configuration for the LUMIO spacecraft, while the mass and power budgets, including margins at system and subsystem level, are shown in Table 7 and Table 8.

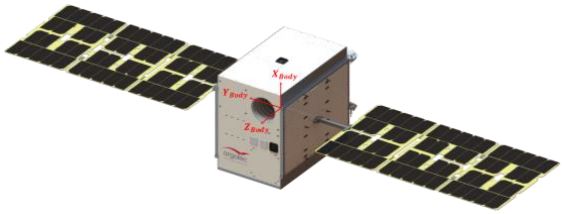

Fig. 13. Spacecraft deployed configuration and Body Reference Frame (BRF)

Table 7. Mass budget of the LUMIO spacecraft.

Subsystem	Mass [kg]	Mass w/ SUB Margins [kg]
PL	4.00	4.80
OBPDP	0.24	0.25
COMM	1.40	1.43
EPS	3.97	4.27
OBC	0.53	0.56
ADCS	2.02	2.13
PS	4.63	5.34
TCS	0.20	0.21
STRUCT	3.90	4.29
Total Dry Mass [kg]		**23.41**
System margin (10%)		2,34
Harness (5% of dry mass)		1.17
PROPELLANT	1.74	1.77
Total Wet Mass w/ SYS margin [kg]		**28.69**

Table 8. Power Budget of LUMIO for each operative mode

	OPERATIVE MODES [W]									
Subsystem	Science	Optical experiment	Prop Heating	Maneuver	COMM	Desaturation	Nominal	Safe	Detumbling	Eclipse
PL	19.0	19.0	0.00	0.00	0.00	0.00	0.00	0.00	0.00	0.00
OBPDP	5.78	5.78	0.00	0.00	0.00	0.00	0.00	0.00	0.00	0.00
COMM	14.19	14.19	14.19	14.19	39.6	14.19	14.19	14.19	14.19	14.19
EPS	10.9	10.9	10.9	10.9	10.9	10.9	9.33	9.33	11.03	9.33
OBC	5.78	5.78	5.78	5.78	5.78	5.78	5.78	5.78	5.78	5.78
AOCS - ADCS PACK	2.91	2.91	2.91	2.91	2.91	2.91	2.91	2.91	7.97	2.91
PS	1.83	1.83	25.49	108.23	1.83	103.51	1.83	1.83	1.83	1.83
TCS	3.15	3.15	0.00	0.00	0.00	0.00	15.75	15.75	0.00	23.10
Required Power w/o Primary Loss	66.71	66.71	62.36	152.81	64.15	148.00	52.37	52.37	44.31	59.87
Total Required Margined Power	88.94	88.94	83.72	192.27	85.87	186.49	71.74	71.74	53.17	71.85
Max Available Power	98.76	98.76	98.76	98.76	98.76	98.76	98.76	98.76	0.00	0.00
Power Margin	6.59	6.59	14.08	-94.47	9.66	-90.96	27.02	27.02	-53.17	-71.85

7. Conclusion

The primary science goal of LUMIO mission is to observe meteoroid impacts on the lunar farside to study the characteristics of meteoroids and to improve the meteoroid models. This will improve the understanding of the meteoroid fluxes in the Solar System, which is crucial for future human outposts on the Moon. The LUMIO mission complements ground-based observations with remote space-based observations, so improving the lunar situational awareness. The mission utilizes a 12U form-factor CubeSat which carries the LUMIO-Cam, an optical instrument capable of detecting light flashes in the visible spectrum to continuously monitor and process the data. The mission implements a novel orbit design and latest CubeSat technologies to serve as a pioneer in demonstrating how CubeSats can become a viable tool for deep space science and exploration. LUMIO is one of the two winners of ESA's LUCE SYSNOVA competition. The project has successfully passed PDR and is now approaching Phase C. LUMIO is implemented within the General Support Technology Programme (GSTP) through the support of the national delegations of Italy (ASI), United Kingdom (UKSA), Sweden (SNSA) and Norway (NOSA).

Acknowledgments

This work has been conducted under ESA Contract No. 4000139301/22/NL/AS within the General Support Technology Programme (GSTP) through the support of the national delegations of Italy (ASI) and Norway (NOSA).

References

[1] Z. Ceplecha et al., Meteor Phenomena and Bodies, Sp. Sci. Rev., vol. 84, no. 3, pp. 327–471, 1998.

[2] P. Brown, R. E. Spalding, D. O. ReVelle, E. Tagliaferri, and S. P. Worden, The flux of small near-Earth objects colliding with the Earth, Nature, vol. 420, no. 6913, pp. 294–296, 2002.

[3] J. L. Ortiz et al., Detection of sporadic impact flashes on the Moon: Implications for the luminous efficiency of hypervelocity impacts and derived terrestrial impact rates, Icarus, 184, pp. 319–326, 2006.

[4] T. V Gudkova, P. H. Lognonné, and J. Gagnepain-Beyneix, Large impacts detected by the Apollo seismometers: Impactor mass and source cutoff frequency estimations, Icarus, vol. 211, no. 2, pp. 1049–1065, 2011

[5] R. M. Suggs, D. E. Moser, W. J. Cooke, and R. J. Suggs, The flux of kilogram-sized meteoroids from lunar impact monitoring, Icarus, vol. 238, Supplement C, pp. 23–36, 2014.

[6] J. Oberst et al., The present-day flux of large meteoroids on the lunar surface--A synthesis of models and observational techniques, Planet. Space Sci., vol. 74, pp. 179–193, 2012.

[7] S. Bouley et al., Power and duration of impact flashes on the Moon: Implication for the cause of radiation, Icarus, vol. 218, no. 1, pp. 115–124, 2012.

[8] L. R. Bellot Rubio, J. L. Ortiz, and P. V Sada, Luminous Efficiency in Hypervelocity Impacts from the 1999 Lunar Leonids, Astrophys. J. Lett., vol. 542, pp. L65--L68, 2000.

[9] R. M. Suggs, W. J. Cooke, R. J. Suggs, W. R. Swift, and N. Hollon, The NASA Lunar Impact Monitoring Program, Earth. Moon. Planets, vol. 102, no. 1, pp. 293–298, 2008.

[10] A. Z. Bonanos et al., NELIOTA: ESA's new NEO lunar impact monitoring project with the 1.2m telescope at the National Observatory of Athens, in Proceedings of the International Astronomical Union, 2015, vol. 10, no. S318, pp. 327–329.

[11] F. Topputo et al., Lunar Meteoroid Impacts Observer. 2016.

[12] D. A. Dei Tos and F. Topputo, On the advantages of exploiting the hierarchical structure of astrodynamical models, Acta Astronaut., vol. 136, pp. 236–247, 2017.

[13] D. A. Dei Tos and F. Topputo, Trajectory refinement of three-body orbits in the real solar system model, Adv. Sp. Res., vol. 59, no. 8, pp. 2117–2132, 2017.

[14] N. P. Dwivedi, Deterministic optimal maneuver strategy for multi-target missions, J. Optim. Theory Appl., vol. 17, no. 1, pp. 133–153, 1975.

[15] K. C. Howell and H. J. Pernicka, Stationkeeping method for libration point trajectories, J. Guid. Control Dyn., vol. 16, p. 151, 1993.

[16] K. Oguri et al., EQUULEUS mission analysys: design of the science orbit phase, in 26th International Symposium on Space Flight Dynamics, 2017, no. 72, pp. 1–7.

[17] V. Franzese, P. Di Lizia, and F. Topputo, Autonomous Optical Navigation for the Lunar Meteoroid Impacts Observer, Journal of Guidance, Control, and Dynamics, 2019, DOI: 10.2514/1.G003999

[18] SRE-PA & D-TEC staff, Margin philosophy for science assessment studies, 2012.

[19] C. H. Acton Jr, Ancillary data services of NASA's navigation and ancillary information facility, Planet. Space Sci., vol. 44, no. 1, pp. 65–70, 1996.

[20] C. H. Acton Jr, N. Bachman, B. Semenov, and E. Wright, A look towards the future in the handling of space science mission geometry, Planet. Space Sci., vol. 150, pp. 9–12, 2018.

[21] Oshima, K. et al., Low-energy transfers to the Moon with long transfers time, in: Celestial Mechanics and Dynamical Astronomy 131 (2019), pp. 1-19.

[22] Giordano, C., Martinelli, A., Buonagura, C., Merisio, G., Franzese, V., & Topputo, F. (2024). Trajectory Design and Analysis of the LUMIO CubeSat. In AIAA Scitech 2024 Forum (pp. 1-12). AIAA.

[23] Panicucci, P., Piccolo, F., Rizza, A., Merisio, G., Topputo, F., & Walker, R. (2024). Vision-Based Navigation for the LUMIO CubeSat Mission. In 46th AAS Guidance, Navigation and Control Conference (pp. 1-20).

[24] Panicucci, P., Piccolo, F., Borgia, S., Rizza, A., Franzese, V., & Topputo, F. (2023). Current status of the lumio autonomous optical navigation experiment. In 12th International Conference on Guidance, Navigation & Control Systems (GNC) and 9th International Conference on Astrodynamics Tools and Techniques (ICATT) (pp. 1-15).